Advanced Energy Production, Exchange and Transport Technologies for Global-Warming Suppression

Shuichi TORII

Department of Mechanical System Engineering, Kumamoto University
torii@mech.kumamoto-u.ac.jp

***Abstract*- The aim of the present study is to introduce the thermal production from the biomss, the heat exchange of its production to the working fluid, and higher efficiency thermal fluid transport and the corresponding modification and advanced method. It is found that (i) the production of N_2O is suppressed in the lower mix ratio region, i.e., under lean burn condition, (ii) overall heat transfer coefficient for herringbone plate is higher than the other plate shapes and an amplification of frictional pressure drop is substantially suppressed for the separate herringbone plate, and (iii) enhancement heat transfer performance is caused by suspending nanoparticles in pure working fluid.**

Keywords- Biomass; Plate Heat Exchanger; Nanofluid; Combustion; Convective Heat Transfer

I. INTRODUCTION

Biomass is a renewable energy source because the energy that it contains comes from the sun. Through the process of photosynthesis, chlorophyll in plants captures the sun's energy by converting carbon dioxide from the air and water from the ground into carbohydrates, complex compounds composed of carbon, hydrogen, and oxygen. When these carbohydrates are burned, they turn back into carbon dioxide, a greenhouse gas and water and release the sun's energy they contain. The thermal production is transferred to the other material, i.e., the working fluid through the heat exchanger.

Plate heat exchanger (PHE) which is employed as evaporator and condenser, is widely used in many industrial applications, because its performance is comparatively higher among the various existing heat exchangers. PHE consists of the frame, the gasket, and the thin plate whose shape is a key factor for the heat transfer enhancement. Heat transfer performance of PHE is enhanced by using turbulence promoters in channel because of amplification of turbulence, while substantial increase in frictional pressure drop causes. Thus the plate surface patterns in PHE are required to promote heat transfer performance and to suppress the frictional pressure drop simultaneously. The thermal fluid exchanged by the heat exchanger is efficiently transported to the other place through the channel etc.

Fluid including nanoparticles is referred to as nanofluid, which is a term proposed by Choi [1]. The term ‘nanofluid’ refers to a two-phase mixture with its continuous phase being generally a liquid and the dispersed phase constituted of ‘nanoparticles’ i.e., extremely fine metallic particles of size below 100 nm. In other words, the large surface-area-to-volume ratio also increases the stability of the suspensions. Thus, the nanofluid becomes a new promising heat transfer fluid in a variety of application cases. For example, the thermal properties of such a nanofluid appear to be well above those of the base-fluid and particularly, the suspended nanoparticles remarkably increase the thermal conductivity of the mixture [2, 3] and improve its capability of energy exchange.

In the preset study, the thermal production from the biomass, the heat exchange of its production to the working fluid, and higher efficiency thermal fluid transport are introduced and the corresponding modification and advanced method are described.

II. EXPERIMENTAL APPRATUS AND EXPERIMENTAL METHOD

A. Thermal Production from Biomass

Figure 1 depicts a schematic of the experimental apparatus, which consists of air compressor, flow meter, liquid and oil storage tanks and effervescent atomizer. Air compressor is adopted to generate the waste liquid and waste oil flows. Waste liquid and waste oil are continuously and independently supplied to effervescent atomizer from each pressurized storage tank, respectively. Here, the effervescent atomizer implies the injection nozzle developed in the present study. A few valves, pressure gauges, pressure regulators and flow meters are located in the feed line to provide the desired operating conditions. The nozzle is fixed on the caster so as to form the horizontal injection configuration of a mixture of waste liquid and waste oil. The injected mixture is ignited by the tiny burner located in the front of the nozzle, resulting in the formation of the horizontal diffusion flame. Figure 2 illustrates the experimental apparatus employed here. It consists of five main components: injection nozzle which jets the mixture of waste oil and waste liquid, a pilot burner for ignition, combustion furnace, cyclone separator, and scrubber. The mixture of waste oil and waste liquid jetted from the exit nozzle is ignited by a pilot burner and forms flame

in the combustion furnace. Combustion gas is exhausted from the exhaust port behind the furnace, goes into the cyclone separator, and is cooled by the rapid volume expansion. The cooled combustion gas is extracted with a syringe. At the same time, solids contained in the cooled gas, i.e., ashes are separated and gathered in receptacle at the bottom of the separator. An uncertainty analysis [4] yields the following results: the uncertainty for the fluid flow rates is estimated to be $\pm 2.5\%$ and that of the combustion gas measurement is $\pm 1.0\%$.

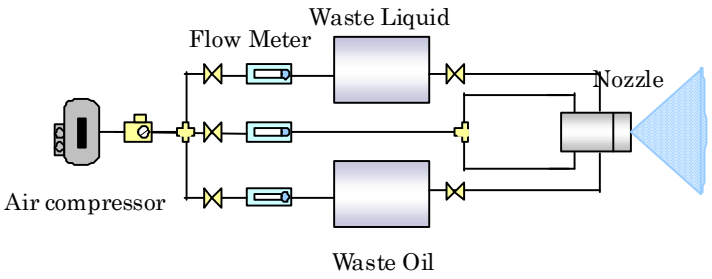

Fig. 1 Schematic diagram of the injection apparatus

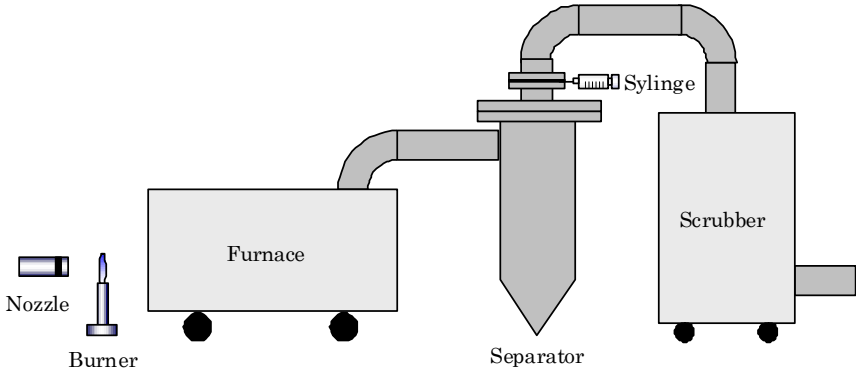

Fig. 2 Experimental apparatus and extraction method of combustion gases

B. Optimum Plate in Plate Exchanger

Figure 3 depicts the experimental apparatus which consists of test section, hot water loop and cold water loop. Water is used as the working fluid in the single plate heat exchanger. Thermal energy of the hot water is transferred to that of the cold one through the titanium plate in the test section. Here hot and cold water is supplied by the independent loops, i.e., hot and cold water loops, respectively. The hot and cold water loops consist of a pump, a tank, three valves and a flow meter, respectively. The water tank in the hot water loop is heated by a pipe heater for adjusting the working fluid temperature, while the corresponding cold water loop is maintained at the constant temperature with the aid of the chiller-unit.

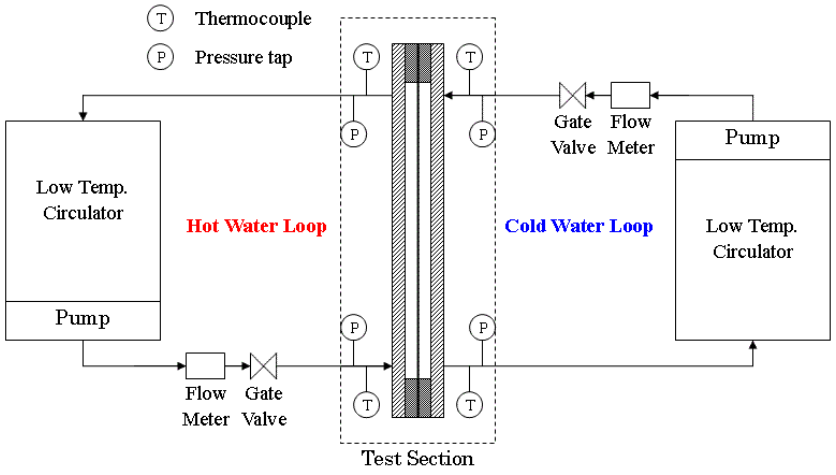

Fig. 3 Schematic of experimental apparatus

Figure 4 illustrates the test section in which thin titanium plate surface with concavity and convexity is sandwiched by two large side walls made of acrylic windows for illumination and observation. The downstream of cold water in one channel is heated by the upstream of hot water in the other channel. The test section is insulated to reduce heat losses. The test section

including the inlet and outlet ports is 500 mm in length and 160 mm in width. The distance between the inlet port and outlet port center is 360 mm and each connection port is 20 mm in diameter. The fluid temperature and pressure drop are measured at the test section inlet and outlet of each channel with the aid of K type thermocouples and pressure gauges, respectively. The overall heat transfer coefficient and frictional pressure drop are estimated by measuring the water temperature, pressure drop and the water flow rate.

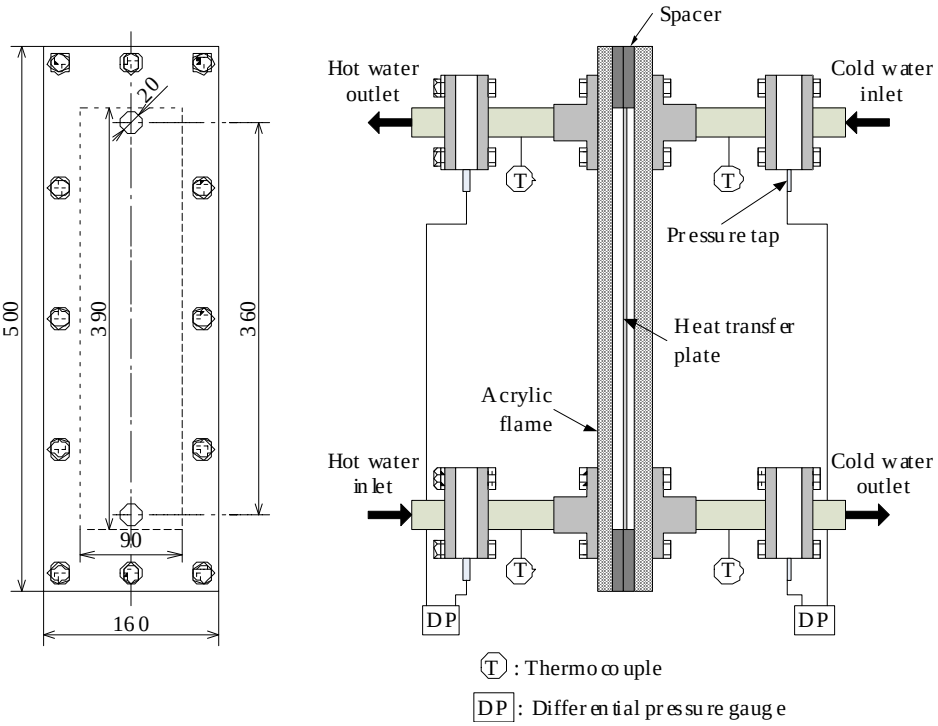

Fig. 4 Test section

C. Heat Transfer Using Nanofluid

Figure 5 depicts the experimental setup which consists of a closed flow loop, a heating unit, a cooling part, and a measuring and control unit. A straight stainless tube with 2000 mm in length, 3.96 mm in inner diameter, and 0.17 mm in thickness which is the test section is employed for measuring the convective heat transfer coefficient. Electrodes for the direct electric current heating are connected at both ends. Notice that the hydrodynamically and thermally fully-developed region is achieved for the test section. In order to suppress heat loss from the test section, a thick thermal insulation material is surrounded around the test tube. The six thermocouples (50 □m in diameter), which are welded on the outer surface of the test tube, are used to measure the local wall temperature along the heated surface of the tube, and the other thermocouples are inserted into the flow at the inlet (T_{in}) and outlet (T_{out}) of the test section to measure the bulk temperature of a working fluid. By using the wall temperature and the input power, the local heat transfer coefficient is estimated.

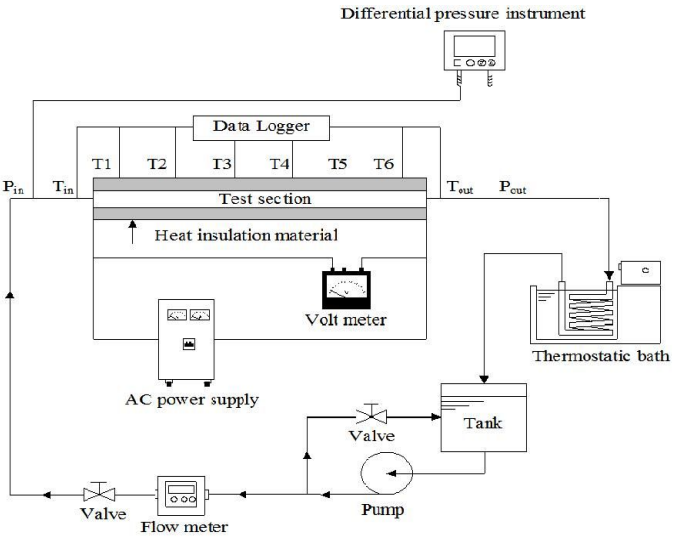

Fig. 5 Experimental apparatus

The measured local wall temperature and heat flux are used to estimate the local Nusselt number Nu_x. The volumetric fraction of 5.0% is tested for alumina (Al_2O_3) nanofluid in the present study. The corresponding pH is 6.66. Ethylene glycol is used as the base liquid, i.e., working fluid. An uncertainty analysis [4] yields the following results: the uncertainty for the flow rate is estimated to be $\pm$2.5%. Since the uncertainty in the physical properties of less than 1% plays only a minor effect on the dimensionless parameter, the average relative uncertainty in Re is estimated to be in the range of $\pm$3.5% or less.

III. RESULTS AND DISCUSSION

A. Thermal Production from Biomass

Figure 6 is the photography of the top view of the flame injected from the horizontal nozzle.

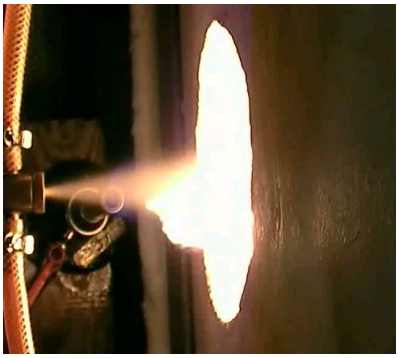

Fig. 6 Photograph of the flame injected from the horizontal nozzle

It is well known that nitrous oxide, N_2O is a major greenhouse gas. It has 310 times more impact per unit weight than carbon dioxide. Thus, despite its low concentration, nitrous oxide is the fourth largest contributor to the greenhouse effect. Control of nitrous oxide is part of efforts to curb greenhouse gas emissions. The relationship of N_2O and O_2 concentrations is illustrated in Fig. 7. There is a linear correlation between N_2O and O_2 and in other words, N_2O is lineally produced with a decrease in O_2.

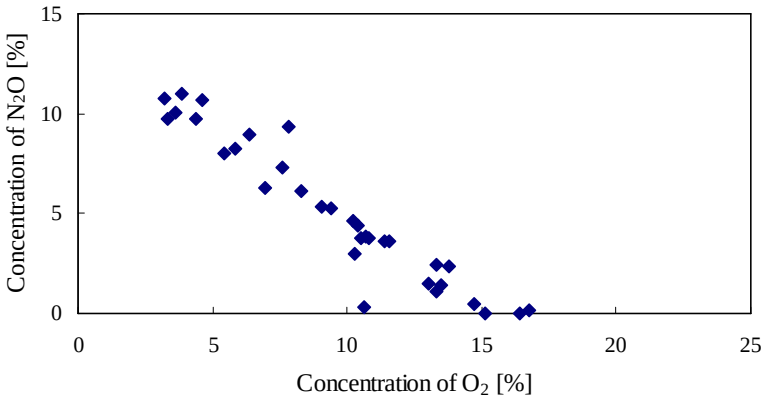

Fig. 7 Relationship between N_2O and O_2

B. Optimum of Plate Shape in Plate Exchanger

Figure 8 depicts the overall heat transfer coefficient for different plate shapes. Here, “Separate herringbone (Block)” and “Plover Pattern (Block)” in figure imply that the angle of convex part is edge. The corresponding coefficients for the herringbone plate and separated herringbone plate are substantially higher than that for flat plate over the whole range of the volume flow rate considered here. This is because the flow is disturbed by the presence of the ribs constructed on the plate, resulting in enhancement of heat transfer performance. The corresponding frictional pressure drop is summarized in Fig. 9. It is observed in Fig. 9 that substantially higher frictional pressure drop occurs on the herringbone plate in comparison with the other plates, particularly the separated herringbone plate. In other words, the friction pressure drop for the separated herringbone plate is lower and is almost the same as that for the plate plat. Note that the open space of middle line of the separated herringbone pattern causes the main fluid flow, resulting in an attenuation of the pressure drop, even if the hydrodynamic diameter is the same.

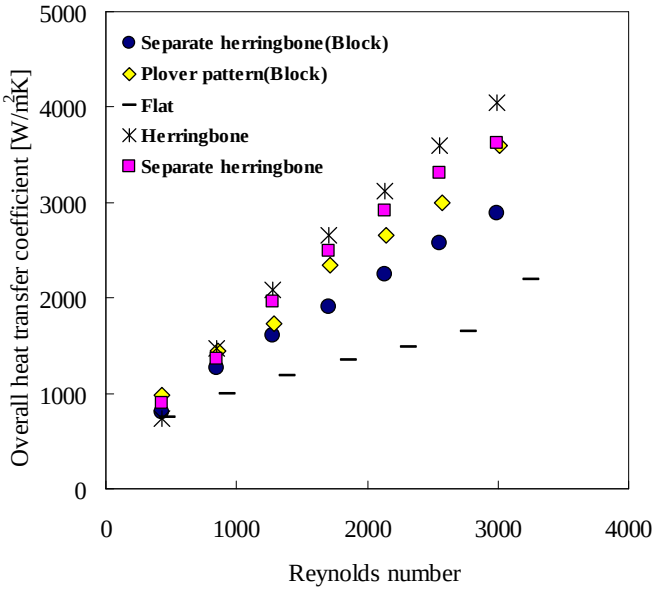

Fig. 8 Overall heat transfer coefficient for different plates

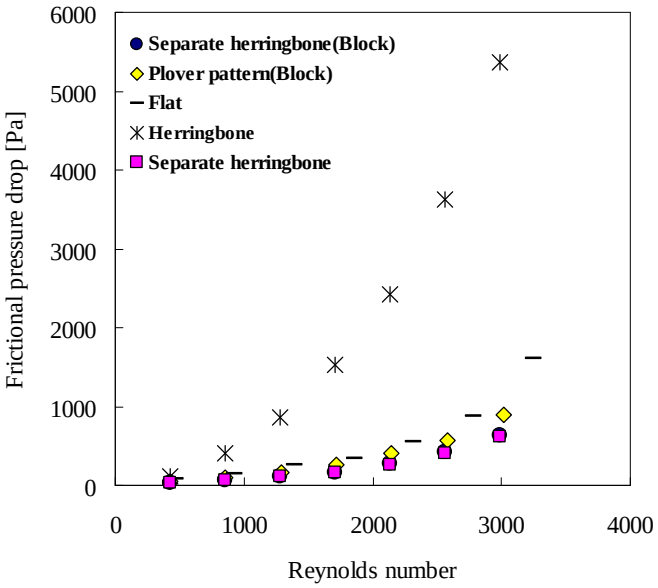

Fig. 9 Friction pressure drop in narrow channel for different plates

The overall performance is illustrated in Fig. 10 in the form of η versus Re, as the plate shape. Figure 10 shows that enhancement of heat transfer performance and suppression of pressure drop are achieved for separate herringbone plate. In contrast, the corresponding performance is substantially low for the herringbone shape. This behavior implies that the enhanced heat transfer performance is achieved as expected, but the overall performance is attenuated over the wide range of the Reynolds number due to substantial amplification of the pressure drop. For reference, the separate herringbone plate is superimposed in Fig. 10.

Here, η is defined as:

$$\eta = (k/\Delta P)/(k_f/\Delta P_f) \quad (1)$$

Here k is the overall heat transfer coefficient, ΔP is the frictional pressure drop and subscript of f represents flat plate. Figure 11 illustrates thermal fluid-flow performance, η, in the same form of Fig. 10 with the gap, g, as the parameter. For reference, the data in Fig. 10 are superimposed in Fig. 11. One observes that as the Reynolds number increases, higher thermal fluid-flow performance is maintained and amplified except the herringbone plate and its trend becomes larger at g=10. That is, substantial heat transfer enhancement and slight amplification of the pressure drop, for separated herringbone plate, are attained between g=4 and g=10 over the wide range of the Reynolds number.

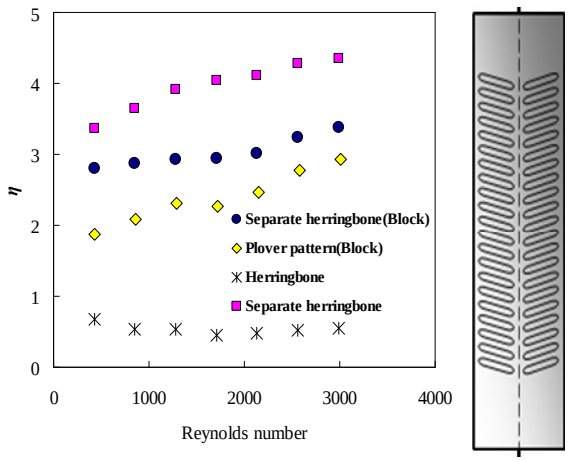

Fig. 10 Variation of h in narrow channel for different plates

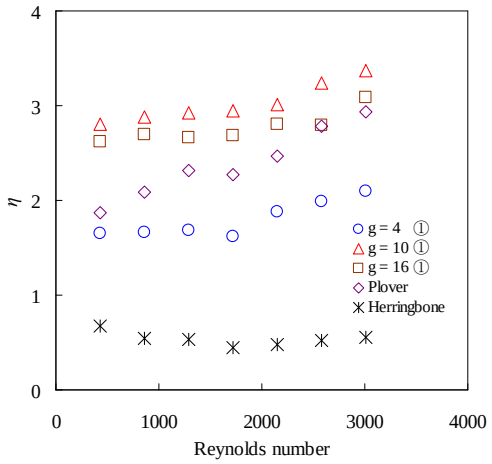

Fig. 11 Variation of h for separated herringbone plate with different gaps

C. Heat Transfer Enhancement with the use of Nanofluid

In the present study, alumina/ethylene glycol nanofluid is employed as the working fluid. The corresponding picture, for reference, is depicted in Fig. 12 which is one of 5 vol.% nanofluid after 60 days. Here, 5 vol.% implies a nanofluid of 5% volume fraction of particles. It is found that the nanofluid employed here maintains stability, because no concentration gradient appears.

Fig. 12 Alumina nanofluid at 5 vol.% of particle volume fraction after 60 days

Heat transfer performance is illustrated in Fig. 13 in the form of Nusselt number Nu versus Reynolds number Re with different working fluids, as a parameter. Here the local heat transfer coefficient at x/D=200, whose location corresponds to the hydrodynamically and thermally fully-developed region, is used to estimate the Nusselt number. For reference, the following Gnielinski equation [5] in the turbulent flow is superimposed as a solid line:

$$Nu = \frac{(f/8)(Re-1000)Pr}{1.07+12.7\sqrt{f/8}\left(Pr^{2/3}-1\right)}, \quad (2)$$

where

$$f = \left[1.82\log_{10}(Re)-1.64\right]^{-2} \quad (3)$$

In the figure, the experimental data for the pure working fluid, i.e., mixture of water and ethylene glycol and nanofluid correspond to diamond and square symbols, respectively. It is found that the results for the pure working fluid agree with the correlation equation and consequently, the experimental apparatus is reliable. One observes that the Nusselt numbers for 5% nanofluid are substantially higher than that for pure working fluid and this trend yields over the Reynolds number region considered here, as shown in Fig. 13. It is postulated that heat transfer enhancement is attributed to the suspension of particles in the working fluid.

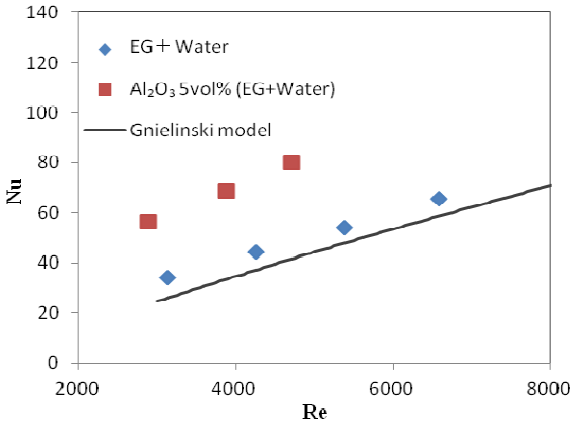

Fig. 13 Nusselt numbers for 5% nanofluid

IV. SUMMARY

The thermal production from the biomass, the heat exchange of its production to the working fluid, and higher efficiency thermal fluid transport have been introduced The results are summarized as follows:

(a) The production of N_2O is suppressed in the lower mix ratio region, i.e., under lean burn condition and in the higher air fuel ratio region. There is an antinomy relation between the production of N_2O and O_2.

(b) Overall heat transfer coefficient for herringbone plate is higher than the other plate shapes employed here. The corresponding frictional pressure drop is substantially high. On the contrary, an amplification of frictional pressure drop is suppressed for the separate herringbone plate. Heat transfer and pressure drop performance are affected by the gap, g, of the separated plate. Substantial heat transfer enhancement and lower pressure drop are achieved at g=10.

(c) Heat transfer performance in the circular tube flow is amplified by suspension of nanoparticles in comparison with that of the working fluid.

REFERENCES

[1] Choi, S. U. S., 1995, "Enhancing thermal conductivity of fluids with nanoparticles," in Developments Applications of Non-Newtonian Flows, FED-vol. 231/MD-vol. 66, ASME: 99-105, edited by D. A. Siginer and H. P. Wang. New York.

[2] Khanafer, K., Vafai, K., and Lightstone, M., "Buoyancy-driven heat transfer enhancement in a two-dimensional enclosure utilizing nanofluid," *International Journal of Heat and Mass Transfer*, vol. 46, pp. 3639-3653, 2003.

[3] S. Lee, S. U. S. Choi, S. Li, and J. A. Eastman, "Measuring thermal conductivity of fluids containing oxide nanoparticles," *Journal of Heat Transfer*, vol. 121, pp. 280-289, 1999.

[4] Kline, S.J. and McClintock, F.A., "Describing Uncertainties in Single-Sample Experiments", *Mechanical Engineering*, pp. 75-76, 1953.

[5] Gnielinski, V., "New equations for heat and mass transfer in turbulent pipe and channel flow," *International Chemical Engineering*, vol. 16, pp. 359-368, 1976.